Current-induced spin-orbit torque in diluted magnetic semiconductors

Hang Li, Xuhui Wang, Fatih Doğan, and Aurelien Manchon*
King Abdullah University of Science and Technology (KAUST), Physical Science and Engineering Division, Thuwal 23955-6900, Saudi Arabia
(Dated: November 6, 2012)

We investigate theoretically the current induced spin-orbit torques in III-V diluted magnetic semiconductors, by combining a six-band Kohn-Luttinger Hamiltonian and a *linear* Dresselhaus spin-orbit coupling. The nonequilibrium spin density and torque are calculated using a Boltzmann equation taking into account transport scattering times obtained from a first-order Born approximation. For two different materials and a wide range of parameters, we scrutinize the angular dependence of the spin torque. We find (1) the spin torque develops a nonlinear dependence on the exchange coupling; (2) a strong correlation between the angular dependence of the torque and the anisotropy of the Fermi surface.

PACS numbers: 72.25.Dc,72.20.My,75.50.Pp

I. INTRODUCTION

In pursuing efficient mechanisms for magnetization switching, spin-transfer torque attracts much attention in the field of spintronics. The Slonczewski-Berger proposal of spin transfer torque adopts a multilayer geometry that comprises two ferromagnetic layers separated by a normal metal spacer,[1,2] where the spin angular momentum is transferred by the carriers from one ferromagnet (polarizer) to the other (free layer), thus inducing excitation on the latter.[3] The spin transfer torque has been achieved in various magnetic structures such as metallic spin valves,[4] magnetic metal tunnel junctions,[5] and especially semiconductors.[6,7]

An alternative approach to accomplish magnetization switching uses spin-orbit interaction that couples orbital angular momentum to spins (with $\hat{\boldsymbol{s}}$ denoting the spin operator) of itinerant charge carriers.[8,9] The spin-orbit Hamiltonian can be generally described by $H_{\rm so} = \hat{\boldsymbol{s}} \cdot \boldsymbol{B}_{\rm so}(\boldsymbol{k})$, where the effective magnetic field $\boldsymbol{B}_{\rm so}(\boldsymbol{k})$ depends on momentum. Two major types of spin-orbit coupling, Rashba and Dresselhaus, exist in a broad range of materials and hybrid structures: the Rashba-type coupling often finds its existence in multilayer structures without inversion symmetry,[10] the cubic Dresselhaus type ($\boldsymbol{B}_{\rm so}(\boldsymbol{k}) \propto k^3$) emerges in zinc-blende crystals,[11] and strain usually introduces a linear Dresselhaus ($\boldsymbol{B}_{\rm so}(\boldsymbol{k}) \propto k$) spin-orbit coupling.[12] In general, in a conductor where both ferromagnetic exchange and spin-orbit couplings are present, the nonequilibrium spin density generated (through the spin-orbit coupling) by the injected charge current is not fully aligned to the direction of the exchange field, thus giving rise to a torque, the so-called spin-orbit torque, exerted on the magnetization.[13–15] Therefore, a separate polarizer is not needed within such a scheme. Several experiments on magnetization switching in metallic thin films have provided strong indication on the spin torque induced by a Rashba-type spin-orbit coupling, see for example, Ref.16.

Besides metallic systems, diluted magnetic semiconductor (DMS) is an excellent candidate for various spin-torque based applications. DMS ideally integrates, in a single realization, itinerant charge carriers, tunable magnetism and spin-orbit couplings. Recent experiments have shown that magnetization can be reversed by an electric current in strained (Ga,Mn)As films,[13,14] employing exactly the spin-orbit torque. The magnetism of a DMS depends on magnetic anisotropy, which is tunable by applying an electric field, doping or strain engineering.[17–19] Electric fields alter the magnetic anisotropy by changing the carrier concentration.[17] Doping affects strain[18] and the exchange interaction.[20] Experiments in (Ga,Mn)As have shown the amplitude of the spin torque increases by doping phosphor.[15] On one hand, doping in general alters lattice constants, resulting in a change in exchange interaction.[21] On the other hand, doping modifies band structures,[22] leading to a variation in magnetic anisotropy. Meanwhile, by engineering the strain, the direction of the easy axis of the anisotropy field can be rotated from being in-plane to out-of-plane,[19] thus offering an opportunity to further manipulate the magnetism. A tunable bulk inversion asymmetry is another characteristic feature of DMS, which allows generation of (linear) Dresselhaus spin-orbit couplings. Spintronic properties and versatility that DMS have demonstrated in numerous applications[23] make them an outstanding platform to investigate physics related to spin-orbit torque.

Despite a few studies on a similar topic,[9,24] a theoretical understanding of the current-induced spin torque in a DMS is far from comprehensive, which motives the present work. In this article, we focus on several issues that have not been addressed in existing literature and organize the rest of the article as follows. Section II outlines the model and methods on which the due discussion is based. In Sec.III, we discuss a strong correlation between an anisotropic Fermi surface and the angular dependence of the torque. Section IV contributes to effect of the exchange interaction on the spin torque. We highlight not only on the role of the exchange coupling as a mediator between the local and itinerant spin angular momenta, but also on its contribution to the spin-

dependent scattering. In Sec.V we investigate the spin torque as a function of hole concentration. In this paper, we provide a comparative study using two popular DMS candidates: (Ga,Mn)As and (In,Mn)As. Finally, Sec.VI concludes the article.

II. HAMILTONIANS AND METHODS

The system under investigation is a uniformly magnetized single domain DMS film made of, for example (Ga,Mn)As or (In,Mn)As. We assume the system is well below its critical temperature. An electric field is applied along the $\hat{x}$ direction to bring the system out of equilibrium. It is worth pointing out: we consider here a large-enough system to allow us disregard any effects arising due to boundaries and confinement.

We use a *six-band* Kohn-Luttinger Hamiltonian to describe the band structure of the DMS,[21]

$$H_{\rm KL}=\begin{pmatrix} H_{\rm hh} & -c & -b & 0 & \frac{b}{\sqrt{2}} & c\sqrt{2} \\ -c^* & H_{\rm lh} & 0 & b & -\frac{b^*\sqrt{3}}{\sqrt{2}} & -d \\ -b^* & 0 & H_{\rm lh} & -c & d & -\frac{b\sqrt{3}}{\sqrt{2}} \\ 0 & b^* & -c^* & H_{\rm hh} & -c^*\sqrt{2} & \frac{b^*}{\sqrt{2}} \\ \frac{b^*}{\sqrt{2}} & -\frac{b\sqrt{3}}{\sqrt{2}} & d^* & -c\sqrt{2} & H_{\rm so} & 0 \\ c^*\sqrt{2} & -d^* & -\frac{b^*\sqrt{3}}{\sqrt{2}} & \frac{b}{\sqrt{2}} & 0 & H_{\rm so} \end{pmatrix}. \tag{1}$$

Hamiltonian Eq. (1) comprises subspaces of heavy holes (hh), light holes (lh), and spin-orbit splitted bands (so), which are defined as

$$H_{\rm hh}=\frac{\hbar^2}{2m}\left[(\gamma_1+\gamma_2)(k_x^2+k_y^2)+(\gamma_1-2\gamma_2)k_z^2\right], \tag{2}$$

$$H_{\rm lh}=\frac{\hbar^2}{2m}\left[(\gamma_1-\gamma_2)(k_x^2+k_y^2)+(\gamma_1+2\gamma_2)k_z^2\right], \tag{3}$$

$$H_{\rm so}=\frac{\hbar^2}{2m}\gamma_1(k_x^2+k_y^2+k_z^2)+\Delta_{so}. \tag{4}$$

The other parameters appearing in Eq.(1) are defined as

$$b=\frac{\sqrt{3}\hbar^2}{m}\gamma_3 k_z(k_x-ik_y), \tag{5}$$

$$c=\frac{\sqrt{3}\hbar^2}{2m}\left[\gamma_2(k_x^2-k_y^2)-2i\gamma_3 k_x k_y\right], \tag{6}$$

$$d=-\frac{\sqrt{2}\hbar^2}{2m}\gamma_2\left[2k_z^2-(k_x^2+k_y^2)\right], \tag{7}$$

where the phenomenological Luttinger parameters $\gamma_{1,2,3}$ determine the band structures and the effective masses of valence-band holes. Particularly, γ_3 is associated with the anisotropy of energy band structure around the Γ point at $\gamma_2\neq\gamma_3$.[25]

Setting $\gamma_1=1.0$ while $\gamma_2=\gamma_3=0$, the six-band Hamiltonian reduces to a simple free-electron model. If $\gamma_2=\gamma_3\neq 0$, the Fermi surfaces of both minority and majority hole bands become spherical. As we will discuss in Sec.III, the angular dependence of the spin torque develops an interesting correlation with the Fermi surface anisotropy.

The bulk inversion asymmetry allows us to augment the Kohn-Luttinger Hamiltonian by a strain-induced spin-orbit coupling of the Dresselhaus type.[9,13] We assume the growth direction of (Ga,Mn)As is directed along the z-axis, two easy axes are pointed at the x and y, respectively.[26] In this case, the components of the strain tensor ϵ_{xx} and ϵ_{yy} are identical. Consequently, we may have a linear Dresselhaus spin-orbit coupling

$$H_{\rm DSOC}=\beta(\sigma_x k_x-\sigma_y k_y), \tag{8}$$

given β the coupling constant that is a function of the axial strain.[13,27] $\sigma_{x(y)}$ is the Pauli matrix and $k_{x(y)}$ are the corresponding components of the wave vector. The spin-orbit coupling Eq.(8) can be viewed as arising from a momentum-dependent effective magnetic field $\boldsymbol{B}_{\rm D}$ that is pointing at the direction $(-k_x,k_y)$.

In the DMS systems discussed here, we incorporate a mean-field like exchange coupling to enable the spin angular momentum transfer between the hole spin ($\hat{\boldsymbol{s}}$) and the localized (d-electron) magnetic moment $\hat{\boldsymbol{\Omega}}$ of ionized Mn^{2+} acceptors,[21,28]

$$H_{\rm ex}=J_{\rm pd}N_{\rm Mn}S_a\hat{\boldsymbol{\Omega}}\cdot\hat{\boldsymbol{s}} \tag{9}$$

where $J_{\rm pd}$ is the coupling constant. In this article, we keep $J_{\rm pd}$ positive, for the exchange coupling is believed to be antiferromagnetic in (Ga,Mn)As[21] and (In,Mn)As.[29] Here $S_a=5/2$ is the spin of the acceptors. The hole spin operator, in the present six-band model, is a 6×6 matrix.[21] The concentration of the ordered local Mn^{2+} moments $N_{\rm Mn}=4x/a^3$ is given as a function of x that defines the doping concentration of Mn ion. a is the lattice constant.

Therefore, the entire system is described by the total Hamiltonian[9]

$$H_{\rm sys}=H_{\rm KL}+H_{\rm ex}+H_{\rm DSOC}. \tag{10}$$

The applied electric field is not explicitly included in Eq.(10) but to be treated in the framework of linear response.

In order to calculate the spin torque, we proceed to determine the nonequilibrium spin densities in response to an external electric field. In the absence of exchange couplings, such an electrically induced spin polarization has been discussed by Edelstein in an infinite medium,[30] which is often referred in literature as the inverse spin-galvanic effect. A comprehensive analytical derivation of the spin-orbit spin torque using field theory technique or Kubo formalism is possible[24] but beyond the scope of this article. In the linear response regime, by solving the Boltzmann equation and retaining the leading order correction in distribution function which is linear in the electric field E_x, we obtain the nonequilibrium spin density of holes $\boldsymbol{S}$,[9]

$$\boldsymbol{S}=eE_x\frac{1}{V}\sum_{n,\boldsymbol{k}}\frac{1}{\hbar\Gamma_{n,\boldsymbol{k}}}\langle\hat{\boldsymbol{v}}\rangle\langle\hat{\boldsymbol{s}}\rangle\delta(E_{n,\boldsymbol{k}}-E_F). \tag{11}$$

The expectation values of the spin and velocity operators are

$$\langle \hat{\boldsymbol{s}} \rangle = \langle \psi_{n\boldsymbol{k}} | \hat{\boldsymbol{s}} | \psi_{n\boldsymbol{k}} \rangle,$$
$$\langle \hat{\boldsymbol{v}} \rangle = \langle \psi_{n\boldsymbol{k}} | \hat{\boldsymbol{v}} | \psi_{n\boldsymbol{k}} \rangle. \quad (12)$$

The velocity operator is obtained using the Heisenberg equation $\hat{\boldsymbol{v}} = (i/\hbar)[\boldsymbol{r}, H_{\rm sys}]$. Diagonalization of the total Hamiltonian [Eq.(10)] generates the eigenstates $\psi_{n\boldsymbol{k}}$. Index n labels 6 different bands: spin-splitted heavy holes, light holes, and spin-orbit splitted bands. The summation runs over all eigenstates.

One important quantity that determines the nonequilibrium spin density (Eq.(11)) is the scattering rate of hole carriers by Mn ions. We use Fermi's golden rule to calculate the rate,[31]

$$\Gamma^{\rm Mn^{2+}}_{n,\mathbf{k}} = \frac{2\pi}{\hbar} N_{\rm Mn} \sum_{n'} \int \frac{d\boldsymbol{k}'}{(2\pi)^3} \left| M^{\boldsymbol{k},\boldsymbol{k}'}_{n,n'} \right|^2 \times \delta(E_{n,\boldsymbol{k}} - E_{n',\boldsymbol{k}'})(1 - \cos\phi_{\boldsymbol{k},\boldsymbol{k}'}), \quad (13)$$

where $\phi_{\boldsymbol{k},\boldsymbol{k}'}$ is the angle between two wave vectors $\boldsymbol{k}$ and $\boldsymbol{k}'$. The matrix element $M^{\boldsymbol{k},\boldsymbol{k}'}_{n,n'}$ between two eigenstates $(\boldsymbol{k}, n)$ and $(\boldsymbol{k}', n')$ is[28]

$$M^{\boldsymbol{k}\boldsymbol{k}'}_{n,n'} = J_{\rm pd} S_a \langle \psi_{n\boldsymbol{k}} | \hat{\boldsymbol{\Omega}} \cdot \hat{\boldsymbol{s}} | \psi_{n'\boldsymbol{k}'} \rangle - \frac{e^2}{\epsilon(|\boldsymbol{k} - \boldsymbol{k}'|^2 + p^2)} \langle \psi_{n\boldsymbol{k}} | \psi_{n'\boldsymbol{k}'} \rangle. \quad (14)$$

Here ϵ is the dielectric constant of the host semiconductors and $p = \sqrt{e^2 g/\epsilon}$ is the Thomas-Fermi screening wave vector,[32] where g is the density of states at Fermi level. Equation (14) suggests there are two scattering channels contributing to the scattering rate, i.e., the spin-dependent part that is due to the exchange coupling, thus proportional to $J^2_{\rm pd}$, and a spin-independent part that arises from the Coulomb interaction.[33]

We calculate the field-like spin torque by using

$$\boldsymbol{T} = J_{\rm ex} \boldsymbol{S} \times \hat{\boldsymbol{\Omega}}, \quad (15)$$

where $J_{\rm ex} \equiv J_{\rm pd} N_{\rm Mn} S_a$. Technically, by diagonalizing the total Hamiltonian Eq.(10), we obtain the eigenvalues and eigenvectors which are then used to calculate the average values as well as the spin density. A formulation that is similar to the above has been developed to explain anisotropic magnetoresistance[28,34] and analyze magneto-optical properties in the same system.[33] In this article, Eqs.(11)-(15) allow us to study the spin-orbit torques for a wide range of material parameters.

At this stage, we need to emphasize that the interband transitions, arising from distortion in distribution function induced by an applied field, are neglected in our calculation. We believe such an omission is justified for two physical reasons. First of all, in the first-order Born approximation considered here, the intraband scattering is dominant.[9] Second, in a relatively clean system where the energy level broadening induced by impurity scattering is much weaker than the Fermi energy, the interband contribution is considered insignificant.[24]

III. FERMI SURFACE

In this section, we concentrate on the behavior of the spin torque as a function of the Luttinger parameters (γ) that determine the band structures as well as the Fermi sphere anisotropy originate Hamiltonian Eq.(1). In the following, we first focus on the so-called spherical approximation to reveal the role of the difference between majority and minority hole densities. Then we relax the spherical approximation to the most general case characterized by the Fermi surfaces that deviate significantly from a sphere.

A. Spherical Fermi surface

The spherical approximation in this section refers to the particular case $\gamma_2 = \gamma_3$. We plot in Fig.1(a), for different values of γ_2, the torque as a function of the magnetization orientation. The initial magnetization direction is along the $\hat{z}$ direction and the applied electric field is applied along the $\hat{x}$ direction. In such a setup, the effective Dresselhaus field ($\boldsymbol{B}_{\rm D}$) is (anti)aligned to the transport direction of the current, We expect that, in the leading order in β, the nonequilibrium spin density is mostly along the $\hat{x}$ direction too. Therefore, the y-component of the spin torque T_y is dominant since we consider in this article the magnetization direction rotates in the xz-plane.

In Fig.1(a), the torque (T_y) is at its maximum when the azimuthal angle $\theta = 0$ (i.e., $\boldsymbol{B}_{\rm D}$ is perpendicular to magnetization direction) and decreasing monotonically towards its minimum at $\theta = \pi/2$ (i.e., $\boldsymbol{B}_{\rm D}$ is aligned with the magnetization). The spin torque fits well by the curve $T \propto \cos\theta$ with a maximal value that increases by increasing γ_2, when the other parameters are fixed.

We explain this by plotting, in Fig. 1(b)-(d), the Fermi surfaces of the majority and minority hole bands in the $k_x - k_y$ plane. As γ_2 becomes larger, the Fermi radii of the spin-splitted heavy hole band increases, so is the nonequilibrium spin density that is proportional to the population difference between the majority and minority bands. The result is an enhanced spin density, thus a larger torque.

B. Non-spherical Fermi surface

In the most general case $\gamma_2 \neq \gamma_3$, we have a non-spherical Fermi surface with the effect of band warping.[34] An interesting correlation between the Fermi surface anisotropy and spin torque emerges when we plot the torque as a function of the magnetization angles. We shall be reminded that γ_3 is associated with the anisotropy energy at the gamma point.[25] The larger the difference between γ_3 and γ_2, the more the Fermi surface deviates from a sphere.

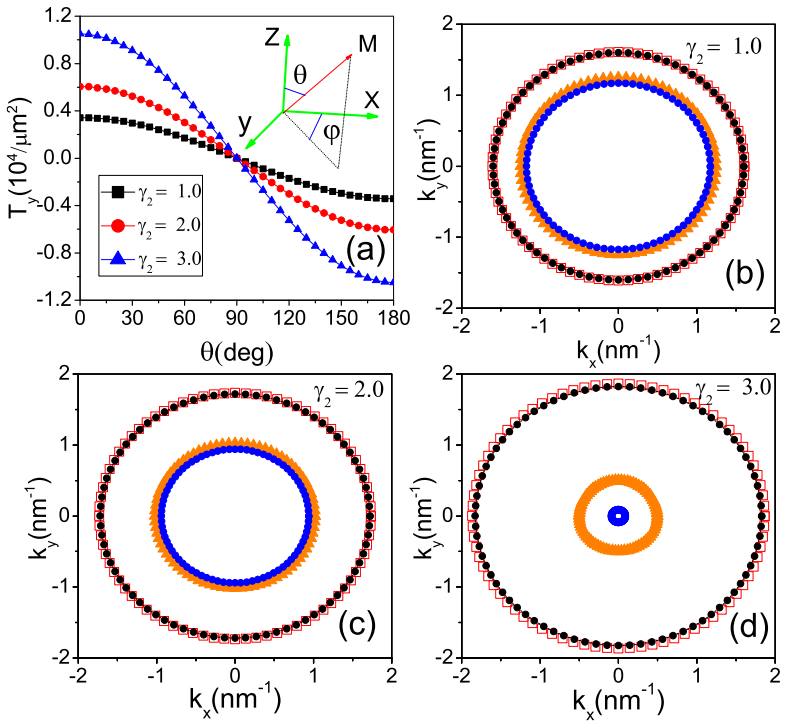

FIG. 1. (Color online). The spherical Fermi surface approximation, i.e., $\gamma_2 = \gamma_3 \neq 0$. Panel (a) The y-component of the spin torque as a function of the magnetization direction for various $\gamma_2(\gamma_3)$ values. θ is the angle between the $\hat{z}$ axis and the magnetization direction. Angle ϕ is between the $\hat{x}$ axis and the projection of magnetization in the xy-plane. In this figure, angle $\phi = 0$. Fermi surface intersection at the $k_z = 0$ plane for (b)$\gamma_2 = \gamma_3 = 1.0$, (c)$\gamma_2 = \gamma_3 = 2.0$, (d)$\gamma_2 = \gamma_3 = 3.0$. The red (empty) square, black dots, orange triangle and blue dots correspond to majority heavy hole, minority heavy hole, majority light hole and minority light hole band, respectively.The others parameters: $\gamma_1 = 6.98$, $x = 0.06$, $J_{\rm pd} = 55$ meV nm^3 and $p = 0.2$ nm^{-3}.

For a given $\gamma_2 = 2.0$ and various values of γ_3, we plot the spin torque as a function of magnetization angle in Fig. 2(a). In this figure, as the Fermi surface deviates from a sphere (i.e., curves corresponding to $\gamma_3 = 1.0$ and $\gamma_3 = 2.93$), the torque shifts away from a simple $\cos\theta$ function. In a comparison to the spherical case, the maximal value of the torque at $\theta = 0$ is lowered as $\gamma_3 \neq \gamma_2$. As Eq.(11) indicates, in the linear response treatment formulated in this article, the magnitude of the spin torque is determined by the transport scattering time and the expectation values of spin and velocity operators of holes. Qualitatively, as the Fermi surface deviates from a sphere, the expectation value $\langle \hat{s}_x \rangle$ of the heavy hole band, contributing the most to the spin torque, is lowered at $\theta = 0$.

We also show in Fig. 2(a) a more interesting behavior of the spin torque: as the Fermi surface warps, the angular dependence of the spin torque shifts away from a simple $\cos\theta$ dependence and develops, in an addition to the $\cos\theta$ envelop function, an oscillation with a period that is shorter than π. The period of these additional oscillation increases as the Fermi surface becomes more anisotropic in k-space, see Fig. 2(b) and (c). To further reveal the effect of band warping on spin torque, we plot $T_y/\cos\theta$ as a function of the magnetization angle in Fig.2(d). When $\gamma_3 = 2.0$ (spherical Fermi sphere), $T_y/\cos\theta$ is a constant, for $T \propto \cos\theta$. When $\gamma_3 = 2.93$ or 1.0, the transport scattering time of the hole carriers starts to develop an oscillating behavior in θ,[34] which eventually contributes to the additional oscillation in the spin torque.

The correlation between the angular dependence of spin torque and the Fermi surface anisotropy found here is similar to the so-called crystalline anisotropic magnetoresistance that emerges from band warping.[34] In fact, such a correlation partially allows a possible mapping between the symmetry properties of Fermi surface and the spin torque that is dynamically measurable.

Material-wise, (In,Mn)As is popular in experiments and device fabrication.[35–37] Although (In,Mn)As is, in terms of exchange coupling and magnetic properties in general, rather similar to (Ga,Mn)As, the difference in band structures, lattice constants, and Fermi energies between these two materials gives rise to different den-

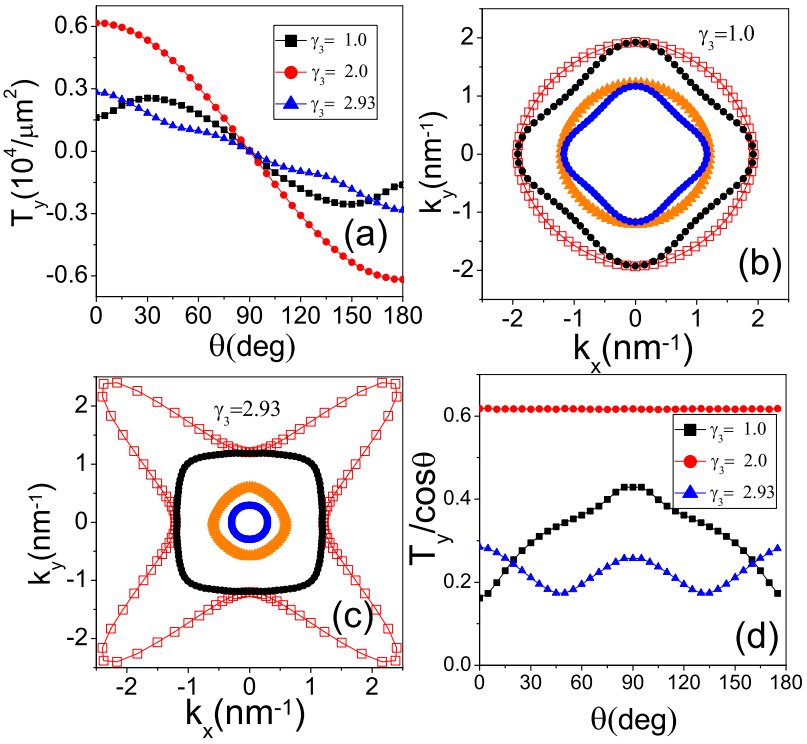

FIG. 2. (Color online) (a)The y-component of the spin torque as a function of magnetization direction. Fermi surface intersection in the $k_z = 0$ plane for (b)$\gamma_3 = 1.0$ and (c)$\gamma_3 = 2.93$. Panel (d) depicts $T_y/\cos\theta$ as a function of magnetization direction. The red (empty) square, black dots, orange triangle and blue dots correspond to majority heavy hole, minority heavy hole, majority light hole and minority light hole, respectively. The others parameters are $(\gamma_1, \gamma_2) = (6.98, 2.0)$, $J_{\rm pd} = 55$ meV nm^3 and $p = 0.2$ nm^{-3}.

sity of states, strains, and transport scattering rates. We plot in Fig.3 the spin torque (T_y) as functions of θ for both (Ga,Mn)As and (In,Mn)As. The following parameters are used in the calculation: the spin-orbit coupling parameter β is found to vary, from $1-5$ meV nm;[38] the exchange coupling constant $J_{\rm pd} = 55$ meV nm^3 for (Ga,Mn)As[39] and 39 meV nm^3 for (In,Mn)As.[40] For both materials, the spin torque decrease monotonically as the angle θ increases from 0 to $\pi/2$. Throughout the entire angle range $[0, \pi]$, the amplitude of the torque in (In,Mn)As is larger than that in (Ga,Mn)As. We attribute this to two effects: (1) the spin-orbit coupling constant β in (In,Mn)As is about twice as larger than that in (Ga,Mn)As; (2) for the same hole concentration, the Fermi energy of (In,Mn)As is higher than that of (Ga,Mn)As.

IV. EXCHANGE INTERACTION

In our model, the spin torque depends not only on the properties of Fermi surface but also on the exchange coupling. From this aspect, our results are in agreement with the findings in Ref.24.

Within the linear response formalism, i.e., Eq.(11), the $p-d$ type exchange coupling makes two contributions to the spin torque. First, the exchange coupling is one of the factors that determine the energy eigenvalue of the total Hamiltonian, separating the majority and minority spin bands and contributing to the expectation value of the spin operator, and thus to the spin torque. The larger $J_{\rm pd}$ becomes, the larger is the energy splitting between majority and minority holes. Second, the exchange coupling contributes to the spin-dependent part of the transport scattering rate (time). A large $J_{\rm pd}$ leads to a short transport time. Therefore, we expect the competition between such two contributions eventually gives rise to a spin torque that depends *nonlinearly* on the exchange coupling $J_{\rm pd}$.

In Fig. 4(a), T_y component of the spin torque is plotted as a function of the exchange coupling $J_{\rm pd}$, for different values of β. In the weak exchange coupling regime, the electric generation of nonequilibrium spin density dominates, then the leading role of exchange coupling is defined by its contribution to the transport scattering rate. We provide a simple qualitative explanation on such a peculiar $J_{\rm pd}$ dependence. Using a Born approximation, the scattering rate due to the $p-d$ interaction is proportional

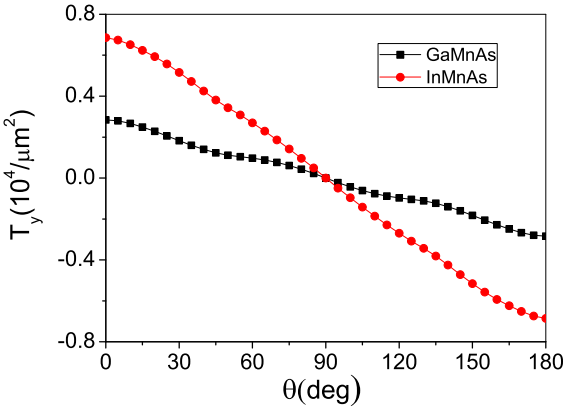

FIG. 3. (Color online) Torque T_y as a function of the magnetization direction for (Ga,Mn)As (black square) and (In,Mn)As (red dots). For (Ga,Mn)As, $(\gamma_1, \gamma_2, \gamma_3) = (6.98, 2.0, 2.93)$; for (In,Mn)As, $(\gamma_1, \gamma_2, \gamma_3) = (20.0, 8.5, 9.2)$. The strength of the spin-orbit coupling constant is: for (Ga,Mn)As, $\beta = 1.6$ meV nm; for (In,Mn)As, $\beta = 3.3$ meV nm.

to $1/\tau_J = bJ_{\rm pd}^2$, where parameter b is $J_{\rm pd}$- independent. When the nonmagnetic scattering rate $1/\tau_0$ is taken into account, i.e., the Coulomb interaction part in Eq.(14), the total scattering time in Eq.(11) can be estimated as

$$\frac{1}{\hbar\Gamma} \propto \frac{1}{bJ_{\rm pd}^2 + \frac{1}{\tau_0}}, \tag{16}$$

which contributes to the torque by $T \propto J_{\rm pd}/(\hbar\Gamma)$. This explains the transition behavior, i.e., increases linearly then decreases, in the not-so-large $J_{\rm pd}$ regime in Fig.4.

As the exchange coupling further increases, Eq.(16) is dominated by the spin-dependent scattering, therefore the scattering time $1/\hbar\Gamma \propto 1/J_{\rm pd}^2$. Meanwhile, the energy splitting due to exchange coupling becomes significant, thus $\langle \hat{\boldsymbol{s}} \rangle \propto J_{\rm pd}$. In total, the spin torque is insensitive to $J_{\rm pd}$, explaining the flat curve in the large exchange coupling regime.

In Fig. 4(b), we plot the influence of the exchange coupling on the spin torque for two materials. In (In,Mn)As, mainly due to a larger Fermi energy in a comparison to (Ga,Mn)As, the peak of the spin torque shifts towards a larger $J_{\rm pd}$. The amplitude of torque in (In,Mn)As is clearly larger, arising from a more robust spin-orbit coupling.

V. HOLE CARRIER CONCENTRATION

The possibility to engineer the electronic properties by doping is one of the defining features that make DMS promising for applications. Here we focus on the doping effect which allows the spin torque to vary as a function of hole carrier concentration.

In Fig. 5(a), the torque is plotted as a function of the hole concentration for different β parameters. With the

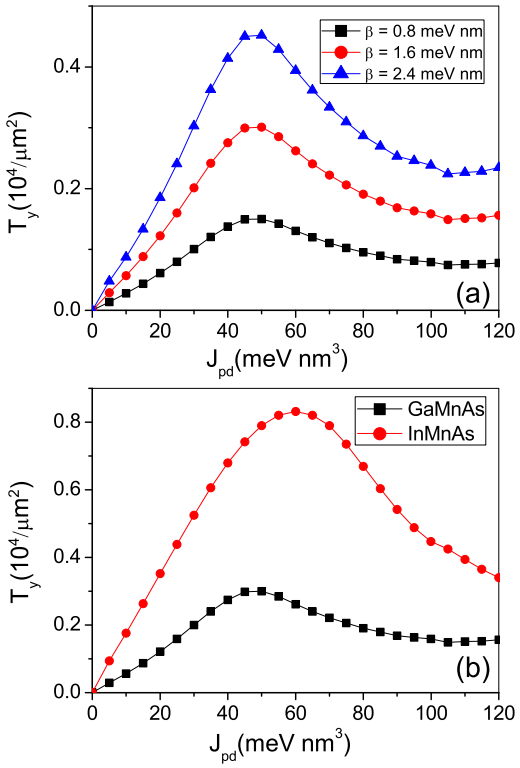

FIG. 4. (Color online) The T_y component of the spin torque as a function of exchange coupling $J_{\rm pd}$. (a) T_y versus $J_{\rm pd}$ at various values of β, for (Ga,Mn)As. (b) T_y versus $J_{\rm pd}$, for both (Ga,Mn)As and (In,Mn)As. The magnetization is directed along the z-axis ($\theta = 0$). The other parameters are the same as those in Fig.3.

increase of the hole concentration, the torques increase due to the enhanced Fermi energy. At a small β (weak spin-orbit coupling), the torque as a function of the hole concentration (p) follows roughly the $p^{1/3}$ curve as shown in the inset in Fig. 5(a). The spherical Fermi sphere approximation and a simple parabolic dispersion relation allow an analytical expression for the spin torque, i.e., in the leading order in β and $J_{\rm pd}$,

$$T = \frac{m^*}{\hbar}\frac{\beta J_{\rm pd}}{E_F}\sigma_{\rm D} \tag{17}$$

where m^* is the effective mass. The Fermi energy E_F and the Drude conductivity are given by

$$E_F = \frac{\hbar^2}{2m^*}(3\pi^2 p)^{2/3},\ \sigma_D = \frac{e^2\tau}{m^*}p, \tag{18}$$

where τ is the transport time. The last two relation immediately gives rise to $T \propto p^{1/3}$. In the six-band model, the Fermi surface deviates from a sphere and as the value of β increases, the spin-orbit coupling starts to modify the density of state. Both effects render the torque versus hole concentration curve away from the $p^{1/3}$ dependence.

In Fig. 5(b), we depict the torque as a function of hole concentration for mentioned materials. In (In,Mn)As the amplitude of the torque is larger than that of (Ga,Mn)As, given the same hole concentration. We attribute this mainly to a larger Fermi energy in (In,Mn)As.

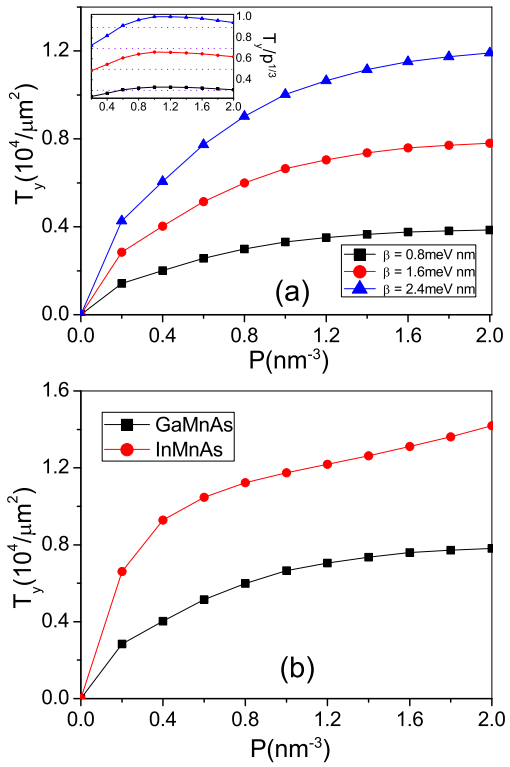

FIG. 5. (Color online) The y-component of the spin torque as a function of hole concentration. (a) The y-component of the spin torque versus hole concentration at different β. (b) spin torque versus hole concentration in (Ga,Mn)As and (In,Mn)As. For (Ga,Mn)As, $J_{\rm pd}$ = 55 meV nm^3; for (In,Mn)As, $J_{\rm pd}$ = 39 meV nm^3. The other parameters are the same as in Fig.4.

VI. SUMMARY AND CONCLUSION

Mediated by itinerant charge carriers, the interplay between a spin-orbit coupling and an exchange splitting gives rise to a spin torque. Using a Kohn-Luttinger Hamiltonian supplemented by a linear Dresselhaus spin-orbit coupling and an exchange interaction, in the framework of linear response, we have studied theoretically the spin torque in two typical III-V diluted magnetic semiconductors (Ga,Mn)As and (In,Mn)As.

Beyond the spherical Fermi sphere approximation that was commonly studied in literature, we found that the spin torque as a function of the magnetization direction has an intriguing correlation with the anisotropy of the Fermi surface. Our calculation also suggests that the spin torque develops a nonlinear dependence on the exchange coupling, which is the result that the exchange coupling not only determines the energy eigenstate but also contributes to the transport scattering rate of the hole carriers. We have also investigated the spin torque as a function of hole concentration. From aspect of material selection, given other parameters the same, the spin torque in (In,Mn)As is usually larger than its counterpart in (Ga,Mn)As.

ACKNOWLEDGMENTS

We are indebted to K. Výborný and T. Jungwirth for numerous stimulating discussions and making Ref.24 available to us. F.D. acknowledges support from KAUST Academic Excellence Alliance Grant N012509-00.

* aurelien.manchon@kaust.edu.sa

[1] J. Slonczewski, J. Magn. Magn. Mater. **159**, L1 (1996).
[2] L. Berger, Phys. Rev. B **54**, 9353 (1996).
[3] D. C. Ralph and M. D. Stiles, J. Magn. Magn. Mater. **320**, 1190 (2008), and references therein.
[4] E. B. Myers, D. C. Ralph, J. A. Katine, R. N. Louie and R. A. Buhrman, Science **285**, 867 (1999).
[5] Y. Huai, F. Albert, P. Nguyen, M. Pakala, and T. Valet Appl. Phys. Lett. **84**, 3118 (2004).
[6] D. Chiba, Y. Sato, T. Kita, F. Matsukura, and H. Ohno, Phys. Rev. Lett **93**, 216602 (2004).
[7] M. Elsen, O. Boulle, J.-M. George, H. Jaffrès, R. Mattana, V. Cros, A. Fert, A. Lemaître, R. Giraud, and G. Faini, Phys. Rev. B **73**, 035303 (2006).
[8] A. Manchon and S. Zhang, Phys. Rev. B **78**, 212405 (2008); Phys. Rev. B **79**, 212405 (2009).
[9] I. Garate and A. H. MacDonald, Phys. Rev.B **80**, 134403 (2009).
[10] Y. A. Bychkov and E. I. Rashba, J. Phys. C: Solid State Phys. **17**, 6039 (1984)
[11] G. Dresselhaus, Phys. Rev. **100**, 580 (1955).
[12] G. L. Bir and G. E. Pikus, *Symmetry and Strain-Induced Effects in Semiconductors* (Wiley, 1974).
[13] A. Chernyshov, M. Overby, X. Liu, J. K. Furdyna, Y. Lyanda-Geller, and L. P. Rokhinson, Nature Phys. **5**, 656 (2009).
[14] M. Endo, F. Matsukura, and H. Ohno, Appl. Phys. Lett. **97**, 222501 (2010).
[15] D. Fang, H. Kurebayashi, J. Wunderlich, K. Výborný, L. P. Zârbo, R. P. Campion, A. Casiraghi, B. L. Gallagher, T. Jungwirth, and A. J. Ferguson, Nature Nanotech. **6**, 413 (2011).

[16] I. M. Miron, G. Gaudin, S. Auffret, B. Rodmacq, A. Schuhl, S. Pizzini, J. Vogel, and P. Gambardella, Nature Mater. **9**, 230 (2010).

[17] H. Ohno, D. Chiba, F. Matsukura, T. Omiya, E. Abe, T. Dietl, Y. Ohno, and K. Ohtani, Nature **408**, 944 (2000).

[18] C. S. King, J. Zemen, K. Olejník, L. Horák, J. A. Haigh, V. Novák, A. Irvine, J. Kučera, V. Holý, R. P. Campion, B. L. Gallagher, and T. Jungwirth, Phys. Rev. B **83**, 115312 (2011).

[19] T. Dietl, H. Ohno and F. Matsukura, Phys. Rev. Lett **63**, 195205 (2001).

[20] M. Elsen, H. Jaffrès, R. Mattana, M. Tran, J.-M. George, A. Miard, and A. Lemaître, Phys. Rev. Lett **99**, 127203 (2007).

[21] M. Abolfath, T. Jungwirth, J. Brum, and A. H. MacDonald, Phys. Rev. B **63**, 054418 (2001).

[22] M. Yahyaoui, C. Testelin, C. Gourdon, and K. Boujdaria, J. Appl. Phys. **111**, 033902 (2012).

[23] T. Jungwirth, J. Sinova, J. Mašek, J. Kučera, and A. H. MacDonald, Rev. Mod. Phys. **78**, 809 (2006).

[24] Liviu P. Zârbo, Karel Výborný, Ion Garate, Jairo Sinova, Dong Fang, Hidekazu Kurebayashi, Andrew J. Ferguson, Antonín Čejchan, and Tomáš Jungwirth, unpublished.

[25] S. L. Chuang, *Physics of Optoelectronic Devices* (Wiley, New York, 1995).

[26] U. Welp, V. K. Vlasko-Vlasov, X. Liu, J. K. Furdyna, and T. Wojtowicz, Phys. Rev. Lett. **90**, 167206 (2003).

[27] B. A. Bernevig and S.-C. Zhang, Phys. Rev. B **72**, 115204 (2005).

[28] T. Jungwirth, M. Abolfath, J. Sinova, J. Kučera, and A. H. MacDonald, Appl. Phys. Lett. **81**, 4029 (2002).

[29] J. van Bree, P. M. Koenraad, and J. Fernández-Rossier, Phys. Rev. B **78**, 165414 (2008).

[30] V. M. Edelstein, Solid State Commun. 73, 233 (1990).

[31] K. Výborný, J. Kučera, J. Sinova, A. W. Rushforth, B. L. Gallagher, and T. Jungwirth, Phys. Rev. B **80**, 165204 (2009).

[32] N. W. Ashcroft and N. D. Mermin, *Solid State Physics* (Saunders College Publishing, Philadelphia, 1976).

[33] Jairo Sinova, T. Jungwirth J. Kučera, and A. H. MacDonald, Phys. Rev. B. **67**, 235203 (2003).

[34] A. W. Rushforth, K. Výborný, C. S. King, K. W. Edmonds, R. P. Campion, C. T. Foxon, J. Wunderlich, A. C. Irvine, P. Vašek, V. Novák, K. Olejník, Jairo Sinova, T. Jungwirth, and B. L. Gallagher, Phys. Rev. Lett. **99**, 147207 (2007).

[35] H. Ohno, H. Munekata, T. Penney, S. von Molnár, and L. L. Chang, Phys. Rev. Lett. **68**, 2664 (1992).

[36] S. Koshihara, A. Oiwa, M. Hirasawa, S. Katsumoto, Y. Iye, C. Urano, H. Takagi, and H. Munekata, Phys. Rev. Lett. **78**, 4617 (1997).

[37] T. Jungwirth, Qian Niu and A. H. MacDonald, Phys. Rev. Lett. **88**, 207208 (2002).

[38] J. Fabian, A. Matos-Abiague, C. Ertler, P. Stano, and I. Zutic, Acta Phys. Slov. **57**, 565 (2007).

[39] H. Ohno, J. Magn. Magn. Mater. **200**, 110 (1999).

[40] J. Wang, Master's thesis (Rice University, Houston, Texas, 2002).